Magneto-Structural Correlations in Macrocyclic Dinickel(II) Complexes: Tuning of Spin Exchange by Varying Stereochemistry and Auxiliary Ligands

Kausik K. Nanda,[1] Ramprasad Das,[1] Laurence K. Thompson,*[2] Krishnan Venkatsubramanian,[3] Parimal Paul,[3] and Kamalaksha Nag*[1]

Department of Inorganic Chemistry, Indian Association for the Cultivation of Science, Calcutta 700 032, India, Department of Chemistry, Memorial University of Newfoundland, St. John's, Newfoundland, Canada A1B 3X7, and Coordination Chemistry Discipline, Central Salt and Marine Chemicals Research Institute, Bhavnagar 364 002, India

Received June 16, 1993®

Variable-temperature (5-300 K) susceptibility measurements carried out for the binuclear nickel(II) complexes of a tetraamino diphenol macrocyclic ligand (H_2L) of compositions $[Ni_2L(H_2O)_4](ClO_4)_2 \cdot 4NH_2CONH_2$ (**1**), $[Ni_2L(NCS)_2(H_2O)_2] \cdot 2Me_2NCHO$ (**2**), $[Ni_2L(MeOH)_2(ClO_4)_2] \cdot 2NHEt_3ClO_4$ (**3**), $[Ni_2L(im)_2](ClO_4)_2$ (**4**), $[Ni_2L(py)_2](ClO_4)_2$ (**5**), and $[Ni_2L(\mu\text{-}O_2CCH_2NH_3)(H_2O)_2](ClO_4)_2 \cdot 2H_2O$ (**6**) are reported. All the complexes behave antiferromagnetically, and the exchange parameter, J, varies in the following way: **1** (-17 cm^{-1}), **2** (-21 cm^{-1}), **3** (-29 cm^{-1}), **4** (-50 cm^{-1}), **5** (-67 cm^{-1}), and **6** (-1 cm^{-1}). The decrease in the value of J from **1** to **3** is attributed to the increase in tetragonal distortion around the metal centers. The change in stereochemistry of nickel(II) to the square pyramidal configuration leads to the significant decrease in the value of J for **4** and **5**. The net effective exchange coupling constant of **6**, in which two orthogonal superexchange pathways are involved, is very small. The X-ray structure of **2** has been determined. The complex crystallizes in the monoclinic space group $P2_1/c$ with a = 10.091(1) Å, b = 7.957(1) Å, c = 24.569(3) Å, β = 92.77(1)°, and Z = 2. The structure was solved by direct methods and refined to R = 0.039 and R_w = 0.042. Complex **2** undergoes two reversible one-electron oxidation steps ($E_{1/2}$ = 0.90, 1.05 V *vs* SCE, Pt/MeCN) with the formation of Ni(II)-Ni(III) and Ni(III)-Ni(III) species.

Introduction

The structural and magnetic properties of binuclear nickel(II) complexes with bridging ligands have received considerable attention over the past two decades. Although no specific magneto-structural correlation has evolved as yet, a few interesting trends have emerged. For example, the chloro-bridged dinickel(II) complexes[4] with square pyramidal coordination are generally antiferromagnetic, while trigonal bipyramidal or six-coordinate systems are ferromagnetic. Ferromagnetic interactions have been found to prevail also in octahedrally coordinated dimeric nickel(II) complexes with end-on azide[5] and isocyanate[6] bridges as well as end-to-end thiocyanate[5a,6] and selenocyanate[7] bridges. By contrast, antiferromagnetic interactions have been reported for end-to-end azido-bridged complexes.[8] When bridging occurs through more complex polynuclear units such as oxalate,[9] squarate,[9a] chloranilate,[10] etc., the magnetic exchange is invariably antiferromagnetic in nature. Antiferromagnetic behavior has also been observed for the phenoxide-bridged macrocyclic binuclear nickel(II) complexes derived from [2 + 2] condensation of 2,6-diformyl-4-methylphenol with 1,3-diaminopropane (H_2L')[11] or its 2-hydroxy derivative.[12]

Unlike planar dihydroxo-bridged copper(II) complexes, where a linear relationship exists[13] between the value of J and the Cu-O-Cu bridge angle, a similar magneto-structural correlation has not been found in nickel(II) complexes because a large number of structural parameters seem to affect the superexchange mechanism in these systems. We have previously shown[14] that although for $[Cu_2L'X_2] \cdot nH_2O$ (X = Cl, Br, I) complexes the Cu-O-Cu bridge angle remains practically unchanged, the value of J varies appreciably with Cl (-360 cm^{-1}), Br (-385 cm^{-1}), and I (-425 cm^{-1}), albeit the axially bound halogen is not involved in the superexchange pathway. It occurred to us that in the case of phenoxide-bridged macrocyclic complexes of nickel(II) variation of axial ligands, especially if that produces changes in stereochemistry, might influence exchange interactions in a significant way. Our previous studies provided access to a few structurally characterized complexes of nickel(II) with the binucleating macrocyclic ligand, H_2L, viz. $[Ni_2L(H_2O)_4](ClO_4)_2$.

® Abstract published in *Advance ACS Abstracts,* February 1, 1994.

(1) Indian Association for the Cultivation of Science.
(2) Memorial University of Newfoundland.
(3) Central Salt and Marine Chemicals Research Institute.
(4) (a) Laskowski, E. J.; Felthouse, T. R.; Hendrickson, D. N. *Inorg. Chem.* **1976**, *15*, 2908. (b) Butcher, R. J.; O'Connor, C. J.; Sinn, E. *Inorg. Chem.* **1979**, *18*, 492. (c) Journeaux, Y.; Kahn, O. *J. Chem. Soc., Dalton Trans.* **1979**, 1575. (d) Jansen, J. C.; Van Koningsveld, H.; Van Ooijen, J. A. C.; Reedijk, J. *Inorg. Chem.* **1980**, *19*, 170. (e) Landee, C. P.; Willet, R. D. *Inorg. Chem.* **1981**, *20*, 2521.
(5) (a) Cortes, R.; Ruiz de Larramendi, T. I.; Lezama, L.; Rojo, T.; Urtiaga, K.; Arriortua, M. I. *J. Chem. Soc., Dalton Trans.* **1992**, 2723. (b) Arriortua, M. I.; Cortes, R.; Lezama, L.; Rojo, T.; Solans, X; Font-Barita, M. *Inorg. Chim. Acta* **1990**, *174*, 263.
(6) Arriortua, M. I.; Cortes, R.; Mesa, J. L.; Lezama, L.; Rojo, T.; Villenueve, G. *Transition Met. Chem. (Weinheim, Ger.)* **1988**, *13*, 371.
(7) (a) Duggan, D. M.; Hendrickson, D. N. *Inorg. Chem.* **1974**, *13*, 2929. (b) Shvelashvili, A. E.; Porii-Koshits, M. A.; Antsyshkina, A. S. *J. Struct. Chem. (Engl. Transl.)* **1969**, *10*, 552. (c) Rojo, T.; Cortes, R.; Lezama, L.; Arriortua, M. I.; Villenueve, G. *J. Chem. Soc., Dalton Trans.* **1991**, 1779.
(8) (a) Pierpont, C. G.; Hendrickson, D. N.; Duggan, D. M.; Wagner, F.; Barefield, E. K. *Inorg. Chem.* **1975**, *14*, 604. (b) Chaudhuri, P.; Guttmann, M.; Ventur, D.; Wieghardt, K.; Nuber, B.; Weiss, J. *J. Chem. Soc., Chem. Commun.* **1985**, 1618.
(9) (a) Duggan, D. M.; Barefield, E. K.; Hendrickson, D. N. *Inorg. Chem.* **1973**, *12*, 985. (b) Battaglia, L. P.; Bianchi, A.; Corradi, A. B.; Garcia-Espana, E.; Micheloni, M.; Julve, M. *Inorg. Chem.* **1988**, *27*, 4174. (c) Bencini, A.; Bianchi, A.; Garcia-Espana, E.; Jeannin, Y.; Julve, M.; Marcelino, V.; Philoche-Leviasalles, M. *Inorg. Chem.* **1990**, *29*, 963. (d) Bencini, A.; Bianchi, A.; Paoli, P.; Garcia-Espana, E.; Julve, M.; Marcelino, V. *J. Chem. Soc., Dalton Trans.* **1990**, 2213.
(10) Pierpont, C. G.; Francesconi, L. C.; Hendrickson, D. N. *Inorg. Chem.* **1977**, *16*, 2367.
(11) (a) Lambert, S. L.; Hendrickson, D. N. *Inorg. Chem.* **1979**, *18*, 2683. (b) Spiro, C. L.; Lambert, S. L.; Smith, T. J.; Duesler, E. N.; Gagne, R. R.; Hendrickson, D. N. *Inorg. Chem.* **1981**, *20*, 1229.
(12) Downard, A. J.; McKee, V.; Tandon, S. S. *Inorg. Chim. Acta* **1990**, *173*, 181.
(13) Crawford, W. H.; Richardson, H. W.; Wasson, J. R.; Hodgson, D. J.; Hatfield, W. E. *Inorg. Chem.* **1976**, *15*, 2107.
(14) Mandal, S. K.; Thompson, L. K.; Newlands, M. J.; Gabe, E. J.; Nag, K. *Inorg. Chem.* **1990**, *29*, 1324.

0020-1669/94/1333-1188$04.50/0

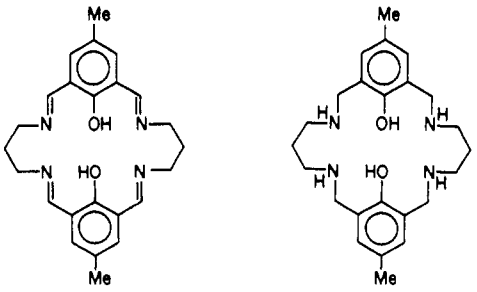

$4NH_2CONH_2$ (**1**),[15] $[Ni_2L(MeOH)_2(ClO_4)_2]\cdot 2NHEt_3ClO_4$ (**3**).[16] $[Ni_2L(py)_2](ClO_4)_2$ (**5**),[17] and $[Ni_2L(\mu\text{-}O_2CCH_2NH_3)(H_2O)_2](ClO_4)_2\cdot 2H_2O$ (**6**).[18] There is change in stereochemistry around the nickel centers from more regular octahedral (**1**) to highly elongated tetragonal (**3**) to square pyramidal (**5**) geometry, and in the six-coordinate complex **6** the carboxylate bridge is perpendicular to the phenoxide bridge. We now report the structure of the thiocyanate complex, $[Ni_2L(NCS)_2(H_2O)_2]\cdot 2Me_2NCHO$ (**2**), and variable-temperature magnetic properties of all the complexes along with the previously characterized imidazole complex $[Ni_2L(im)_2](ClO_4)_2$ (**4**).[17]

Experimental Section

Materials. All chemicals were reagent grade and used as received. The ligand H_2L was prepared as reported earlier,[19,20] as were complexes **1**,[15] **3**,[16] **4**,[17] **5**,[17] and **6**.[18]

Synthesis of $[Ni_2L(NCS)_2(H_2O)_2]\cdot 2Me_2NCHO$ (2). To a methanol solution (50 mL) of $[Ni_2L(MeOH)_2(ClO_4)_2]\cdot 2NHEt_3ClO_4$ (**3**) (1.19 g, 1 mmol) was added solid NaNCS (0.20 g, 2.47 mmol). The wine red solution changed to a sky blue color. After 15 min, 10 mL of acetone was slowly added. On standing, blue crystals of composition $[Ni_2L(NCS)_2(H_2O)_2]\cdot 2Me_2CO$ deposited, which, however, lose crystallinity over a few hours due to the slow release of acetone. Recrystallization of this compound from DMF–MeCN (1:10) afforded the sky blue crystals of **2**. Anal. Calcd for $C_{32}H_{52}N_8O_6S_2Ni_2$: C, 46.52; H, 6.30; N, 13.57. Found: C, 46.34; H, 6.36; N, 13.64.

C, H, and N analyses were performed on a Perkin-Elmer 240C elemental analyzer.

Physical Measurements. Infrared spectra were recorded on a Perkin-Elmer 783 spectrophotometer using KBr disks. Electronic spectra were obtained with a Hitachi U3400 spectrophotometer in the UV–vis and near-IR regions. The electrochemical measurements were performed at room temperature in acetonitrile under O_2-free conditions using a BAS 100B electrochemical analyzer (Bioanalytical Systems). A three-electrode assembly (BAS) comprising a Pt working electrode, a Pt auxiliary electrode, and a saturated calomel reference electrode (SCE) was used. The supporting electrolyte was $[Et_4N][ClO_4]$ (0.1 M), and all solutions were *ca.* 10^{-3} M in complex.

Variable-temperature magnetic susceptibility data were obtained in the range 5–300 K by using an Oxford Instruments superconducting Faraday magnetic susceptibility system with a Sartorius 4432 microbalance. A main solenoid field of 1.5 T and a gradient field of 10 T m^{-1} were employed. Susceptibility data were corrected for diamagnetism (Pascal corrections), for temperature-independent paramagnetism, and for the presence of monomer impurity. $Hg[Co(NCS)_4]$ was used as a calibration standard.

X-ray Crystallography. Crystals of $[Ni_2L(NCS)_2(H_2O)_2]\cdot 2Me_2NCHO$ (**2**) suitable for X-ray diffraction studies were obtained by diffusion of diethyl ether to a DMF solution of the complex. The crystals are blue in color. The diffraction intensities of an approximately 0.21 × 0.18 × 0.20 mm crystal were collected by using a Enraf-Nonius CAD4 diffractometer with Mo Kα radiation (λ = 0.710 69 Å). The cell parameters were obtained by the least-squares refinement of 25 arbitrarily chosen higher order reflections. Crystal stabilities were checked by monitoring intensities of three standard reflections after every 100 reflections, and no significant variations were noted. The intensity data were corrected for Lorentz–polarization effects and for absorption by an emperical method.[21] A total of 3063 reflections were collected in the range $2 \le 2\theta \le 47°$, of which 2467 reflections with $I > 3\sigma(I)$ were used for the structure determination.

The structure was solved by direct and Fourier difference methods using the program MULTAN 82.[22] Hydrogen atoms were either generated using stereochemical constraints or located in the difference Fourier map. The structure was refined by the block-diagonal least-squares technique to final residuals of R and R_w of 0.039 and 0.042, respectively, using weights based on counting statistics {$R = \sum(|F_o| - |F_c|)/\sum|F_o|$; $R_w = [\sum w(|F_o| - |F_c|)^2/\sum w(|F_o|)^2]^{1/2}$}. The final difference map had no peaks greater than 0.43 e Å^{-3}. The scattering factors were taken from ref 23. All calculations were performed with the SDP package[24] for the PDP-11/73 system. A summary of crystal data is given in Table 1, and atomic coordinates are given in Table 2. Lists of

Table 1. Crystallographic Data for $[Ni_2L(NCS)_2(H_2O)_2]\cdot 2(CH_3)_2NCHO$ (**2**)

formula	$C_{32}H_{52}N_8O_6S_2Ni_2$	V, Å^3	1970.4
fw	826.3	Z	2
cryst system	monoclinic	d_{calcd}, g cm^{-3}	1.393
space group	$P2_1/c$	temp, K	293
a, Å	10.091(1)	λ, Å	0.710 69
b, Å	7.957(1)	μ, cm^{-1}	11.4
c, Å	24.569(3)	R^a	0.039
β, deg	92.77(1)	Rw^b	0.042

^{a} $R = \sum(|F_o| - |F_c|)/\sum|F_o|$. ^{b} $R_w = [\sum w(|F_o| - |F_c|)^2/\sum w|F_o|^2]^{1/2}$.

Table 2. Positional and Equivalent Isotropic Thermal Parameters of Non-Hydrogen Atoms (Esd's in Parentheses) for $[Ni_2L(NCS)_2(H_2O)_2]\cdot 2Me_2NCHO$ (**2**)

atom	x	y	z	B_{iso},[a] Å^2
Ni(1)	0.61192(4)	0.13197(6)	0.49360(2)	2.29(1)
S(4)	0.8287(2)	−0.1208(4)	0.34282(8)	9.83(7)
O(5)	0.4975(3)	0.2780(3)	0.5524(1)	3.00(6)
O(6)	0.5716(2)	−0.0719(3)	0.5402(1)	2.53(6)
O(21)	0.6262(3)	−0.7951(4)	0.6497(1)	4.54(8)
N(2)	0.7100(3)	−0.0024(5)	0.4346(2)	3.36(8)
N(15)	0.7837(3)	0.1682(4)	0.5426(1)	2.82(7)
N(19)	0.6126(3)	0.3510(4)	0.4483(1)	2.57(7)
N(23)	0.6348(4)	−0.9867(5)	0.7183(2)	4.5(1)
C(3)	0.7602(4)	−0.0504(6)	0.3965(2)	3.6(1)
C(7)	0.6497(4)	−0.1612(5)	0.5746(2)	2.43(8)
C(8)	0.5985(4)	−0.2923(5)	0.6064(2)	2.81(9)
C(9)	0.6823(4)	−0.3892(6)	0.6403(2)	3.5(1)
C(10)	0.8182(4)	−0.3581(6)	0.6459(2)	4.0(1)
C(11)	0.8669(4)	−0.2254(6)	0.6169(2)	3.7(1)
C(12)	0.7874(4)	−0.1271(5)	0.5813(2)	2.84(8)
C(13)	0.9074(6)	−0.4653(8)	0.6838(3)	6.8(2)
C(14)	0.8559(4)	0.0066(6)	0.5495(2)	3.3(1)
C(16)	0.8789(4)	0.2977(6)	0.5242(2)	3.9(1)
C(17)	0.8117(4)	0.4537(6)	0.5014(2)	3.8(1)
C(18)	0.7454(4)	0.4295(5)	0.4446(2)	3.5(1)
C(20)	0.5486(4)	0.3272(5)	0.3928(2)	3.05(9)
C(22)	0.5781(5)	−0.9100(6)	0.6754(2)	4.0(1)
C(24)	0.5693(7)	−1.1218(8)	0.7463(2)	6.7(2)
C(25)	0.7674(7)	−0.944(1)	0.7371(3)	8.6(2)

^{a} $B_{iso} = {}^4/_3[a^2\beta_{11} + b^2\beta_{22} + c^2\beta_{33} + ab(\cos\gamma)\beta_{12} + ac(\cos\beta)\beta_{13} + bc(\cos\alpha)\beta_{23}]$.

(15) Nanda, K. K.; Das, R.; Venkatsubramanian, K.; Paul, P.; Nag, K. *J. Chem. Soc., Dalton Trans.* **1993**, 2515.
(16) Das, R.; Nag, K. *Inorg. Chem.* **1991**, *30*, 2831.
(17) Nanda, K. K.; Das, R.; Newlands, M. J.; Hynes, R.; Gabe, E. J.; Nag, K. *J. Chem. Soc., Dalton Trans.* **1992**, 897.
(18) Das, R.; Nanda, K. K.; Venkatsubramanian, K.; Paul, P.; Nag, K. *J. Chem. Soc., Dalton Trans.* **1992**, 1253.
(19) (a) Mandal, S. K.; Nag, K. *J. Org. Chem.* **1986**, *51*, 3900. (b) Mandal, S. K.; Thompson, L. K.; Nag, K.; Charland, J.-P.; Gabe, E. J. *Inorg. Chem.* **1987**, *26*, 1391.
(20) The correct melting point of the compound is 145 °C (unsealed capillary).
(21) North, A. C. T.; Phillips, D. C.; Mathews, F. S. *Acta Crystallogr., Sect. A* **1968**, *24*, 351.
(22) Main, P.; Germain, G.; Declercq, J. P.; Woolfson, M. M.; MULTAN-82. A System of Computer Programs for the Automatic Solution of Crystal Structures from X-ray Data. University of York, York, U.K., 1982.
(23) *International Tables for X-Ray Crystallography*; Kynoch Press: Birmingham, England, 1974; Vol. IV.
(24) Enraf-Nonius Structure Determination Package, Enraf-Nonius, Delft, The Netherlands, 1985.

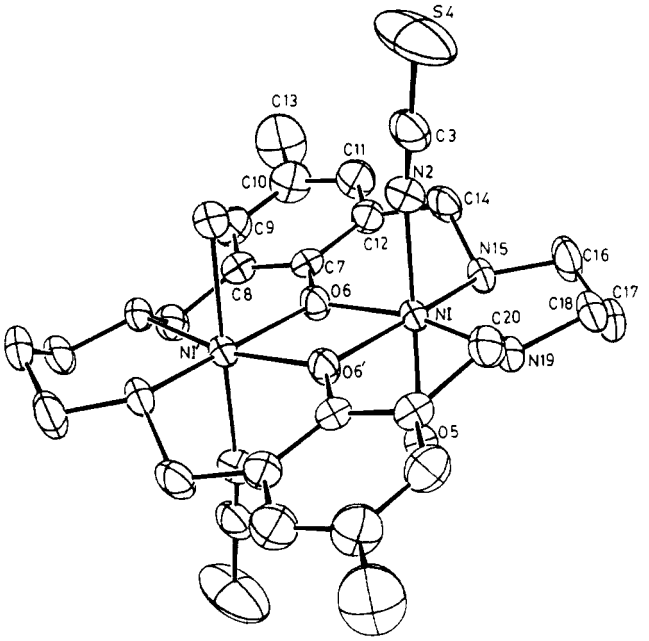

Figure 1. ORTEP diagram of $[Ni_2L(NCS)_2(H_2O)_2]$ (**2**) drawn with the thermal ellipsoids at the 50% probability level. Solvent molecules have been omitted for clarity.

Table 3. Selected Bond Distances (Å) and Angles (deg) for $[Ni_2L(NCS)_2(H_2O)_2]\cdot 2(CH_3)_2NCHO$ (**2**)

Ni···Ni	3.113(3)	Ni–N(2)	2.080(4)
Ni–O(6)	2.032(3)	Ni–O(5)	2.213(3)
Ni–O(6)	2.047(2)	N(2)–C(3)	1.145(6)
Ni–N(15)	2.078(3)	C(3)–S(4)	1.610(5)
Ni–N(19)	2.063(3)		
Ni–O(6)–Ni	99.2(1)	O(5)–Ni–O(6)	83.9(1)
O(6)–Ni–O(6)	80.6(1)	O(5)–Ni–N(19)	85.3(1)
N(15)–Ni–N(19)	99.6(1)	O(5)–Ni–N(2)	176.4(1)
O(6)–Ni–N(15)	88.5(1)	O(6)–Ni–N(19)	168.2(2)
O(6)–Ni–N(19)	90.5(2)	O(6)–Ni–N(15)	167.8(1)
O(6)–Ni–N(2)	95.3(1)	Ni–N(2)–C(3)	167.5(4)
N(2)–Ni–N(15)	93.3(1)	S(4)–C(3)–N(2)	178.9(4)

anisotropic thermal parameters (Table S1), complete bond lengths and angles (Table S2), and hydrogen atom positions (Table S3) are included as supplementary material.

Results and Discussion

Description of the Structure of 2. The ORTEP representation of the $[Ni_2L(NCS)_2(H_2O)_2]$ complex is shown in Figure 1, and interatomic distances and angles relevant to the nickel coordination sphere are given in Table 3. The structure consists of two nickel centers bridged by two phenoxide oxygen atoms with two secondary amine nitrogen donors completing the NiN_2O_2 basal plane. Each of the metal centers achieves a pseudo-octahedral configuration through the axial coordination of thiocyanate ions and water molecules, which are *trans* to each other. Complex **2** has a centrosymmetric structure with the center of inversion at the middle of Ni_2O_2 plane. The macrocyclic donor atoms, N_2O_2, form an exact plane, within 0.02 Å, from which the nickel atom is displaced by 0.127 Å. The two nickel atoms are separated by 3.113(3) Å, with a Ni–O–Ni bridge angle of 99.2(1)°. The bond distances involving the axial ligands are not equal. Although the Ni–NCS distance, 2.080(4) Å, is normal,[25] the Ni–OH_2 distance, 2.213(3) Å, is rather long compared to the range 2.04–2.16 Å reported for various *trans*-aqua octahedral nickel(II) complexes.[25]

In Figure 2 the interatomic distances relevant to the nickel coordination sphere in complexes **1**–**3** (**I**–**III**), **5** (**V**), and **6** (**VI**)

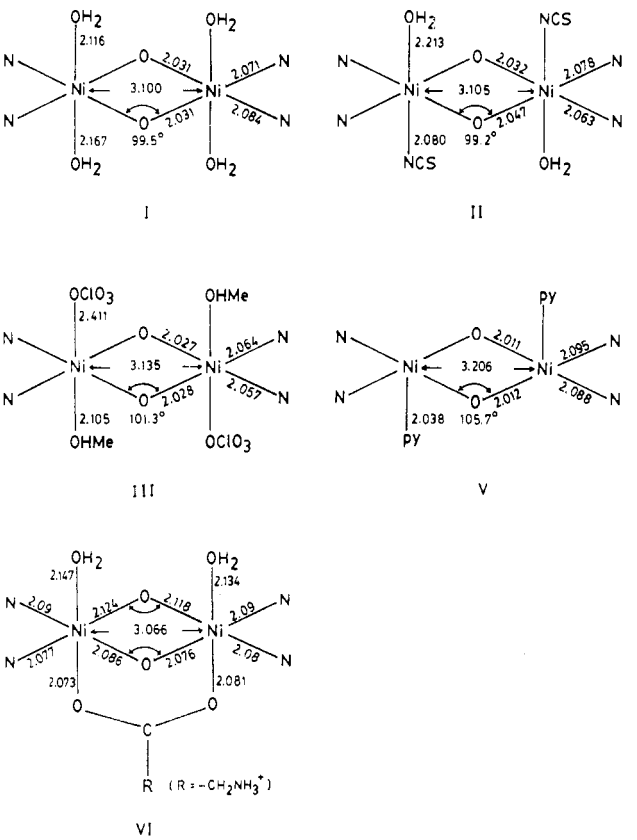

Figure 2. Interatomic distances and angles relevent to the coordination sphere in complexes **1** (**I**), **2** (**II**), **3** (**III**), **5** (**V**), and **6** (**VI**).

are depicted. It may be noted that, except for **VI**, in all the cases Ni–O(phenol) distances (2.025 ± 0.015 Å) and Ni–N(amine) distances (2.08 ± 0.02 Å) show only marginal variations. The average in-planar Ni–O distance in **VI**, 2.10 Å, is much longer. The nickel–nickel separation is smallest in **VI** (3.066 Å) and largest in **V** (3.206 Å), with the others lying between (3.10–3.13 Å). Most importantly, there is a progressive increase in bond lengths of one of the metal–axial donors from **I** to **III**. Structure **V** may be regarded as one in which further elongation has removed this bond from the octahedral array.

The molecular structure of **2** reveals that the carbonyl oxygen, O(21), of DMF is strongly hydrogen bonded to the coordinated water molecule and an amino group of the macrocyclic ligand. Thus, O(21)···O(5) = 2.71 Å, O(5)–H(51)–O(21) = 164.7° and O(21)···N(15) = 3.13 Å, O(21)–H(15)–N(15) = 164.5°. Another NH group of the macrocycle is also involved in hydrogen bonding with O(5), where O(5)···N(19) = 3.15 Å and N(19)–N(19)–O(5) = 147.6°. Surprisingly, the nitrogen atom of the thiocyanate ion is also additionally involved in a hydrogen bonding with the water molecule, where O(5)···N(2) = 3.06 Å and O(5)–H(52)–N(2) = 153.0°.

Spectral and Electrochemical Properties. The infrared spectrum of **2** exhibits two NH stretching vibrations at 3280 and 3240 cm^{-1} and a bending vibration at 1610 cm^{-1} due to the macrocyclic ligand. Although a single NH stretch is expected for the symmetric structure **II**, the splitting of this band into two components may be attributed to the involvement of the amino groups in hydrogen bonding. The compound is further characterized by two strong bands, one at 2060 cm^{-1} due to N-bonded thiocyanate and another at 1650 cm^{-1} (ν(C=O)) due to DMF.

The electronic spectrum of **2** in DMF exhibits six d–d transitions, typical of tetragonal nickel(II) complexes of D_{4h} symmetry and is in agreement with the crystal structure. These absorptions [λ_{max}, nm (ϵ, L mol^{-1} cm^{-1})] occurring at 1300 (7), 1150 (8), 860 (20), 640 (40), 470 sh, and 375 (440) nm can be related to the spin-allowed transitions from $^3B_{1g}$ to ^3E_g, $^3B_{2g}$,

(25) Sacconi, L. *Transition Metal Chemistry*; Carlin, R. L., Ed.; Marcel Dekker: New York, 1968; Vol. IV, p 199.

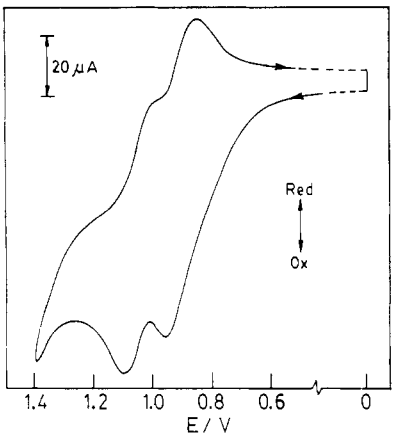

Figure 3. Cyclic voltammogram on a platinum electrode for the oxidation of $[Ni_2L(NCS)_2(H_2O)_2]\cdot 2Me_2NCHO$ (**2**) in acetonitrile at a scan rate of 200 mV s^{-1}.

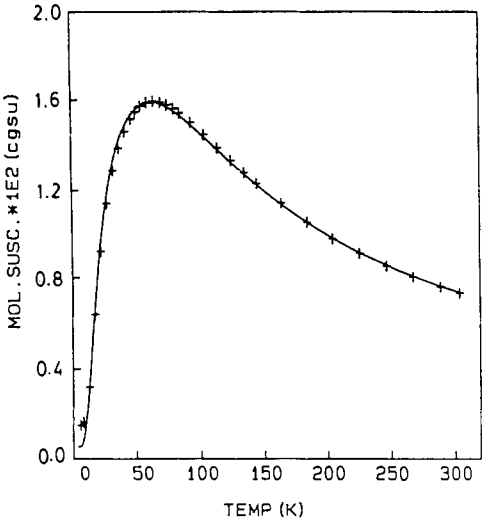

Figure 4. Molar magnetic susceptibility data *vs* temperature for $[Ni_2L(NCS)_2(H_2O)_2]\cdot 2Me_2NCHO$ (**2**). The solid line represents the least-squares fit of the data to the theoretical eq 2 given in the text.

$^3A_{2g}$, ^3E_g, $^3A_{2g}(P)$, and $^3E_g(P)$, respectively. An internal ligand transition absorption is additionally observed at 290 (7400) nm.

Figure 3 shows the cyclic voltammogram for the stepwise oxidation of **2** in acetonitrile (Pt electrode). Two reversible[26] one-electron oxidation steps ($E_{1/2}$ = 0.90, 1.05 V *vs* SCE) involving the formation of $Ni^{II}Ni^{III}$ and $Ni^{III}Ni^{III}$ species are observed. Differential pulse voltammetric measurements also revealed the occurrence of two waves with the same pulse heights at the potentials mentioned above. These potentials are closely comparable to the values, 0.95 and 1.10 V, observed for the oxidation of $[Ni_2L(H_2O)_4]^{2+}$ ion in **1**.[15] The small, but constant, shift of potential for both the redox couples of **2** relative to those of **1** clearly indicates that it is easier to remove electrons in steps by 50 mV from the electrically neutral $[Ni_2L(NCS)_2(H_2O)_2]$ species as compared to the cationic $[Ni_2L(H_2O)_4]^{2+}$ species.

Magnetochemistry. The variable-temperature (5–300 K) magnetic susceptibility data were collected for $[Ni_2L(H_2O)_4](ClO_4)_2\cdot 4NH_2CONH_2$ (**1**), $[Ni_2L(NCS)_2(H_2O)_2]\cdot 2(CH_3)_2NCHO$ (**2**), $[Ni_2L(MeOH)_2(ClO_4)_2]\cdot 2NHEt_3ClO_4$ (**3**), $[Ni_2L(im)_2](ClO_4)_2$ (**4**), $[Ni_2L(py)_2](ClO_4)_2$ (**5**), and $[Ni_2L(\mu\text{-}O_2CCH_2NH_3)(H_2O)_2](ClO_4)_2\cdot 2H_2O$ (**6**). The data are given in Tables S4–S9 (supplementary material) and are illustrated in Figures 4–9.

Usually for binuclear nickel(II) complexes the crystal field splitting of the S = 1 ground state ($^3A_{2g}$ or $^3B_{1g}$) is of the same order of magnitude as the electron spin-exchange integral (J).[27] Accordingly, a magnetic model is used which takes into consideration zero-field splitting (D), intradimer exchange (J), and also an interdimer exchange interaction parameter (zJ'). The spin Hamiltonian (eq 1) includes these terms, and the resulting

$$H = -2J\hat{s}_1\cdot\hat{s}_2 - D(\hat{s}_{1z}^2 + \hat{s}_{2z}^2) - 2zJ'\hat{S}_i\langle\hat{S}_i\rangle - g_i\beta H\hat{S}_i \quad (1)$$

magnetic susceptibility equation, $\chi(g, J, D, zJ')$, derived by Ginsberg *et al.*[28] has been used to fit the magnetic data. The equation has been modified (eq 2) to account for monomeric

$$\chi_M = \chi(g, J, D, zJ')(1-\rho) + \frac{2N\beta^2g^2\rho}{3kT} + N\alpha \quad (2)$$

impurity (ρ represents the fraction of a possible magnetically dilute mononuclear nickel(II) impurity) and temperature-independent paramagnetism ($N\alpha = 8N\beta^2/10Dq$). The symbols N, β, g, and k have their usual meanings. In a few cases the spin Hamiltonian for an isotropic magnetic exchange, $H = -2J\hat{s}_1\cdot\hat{s}_2$,

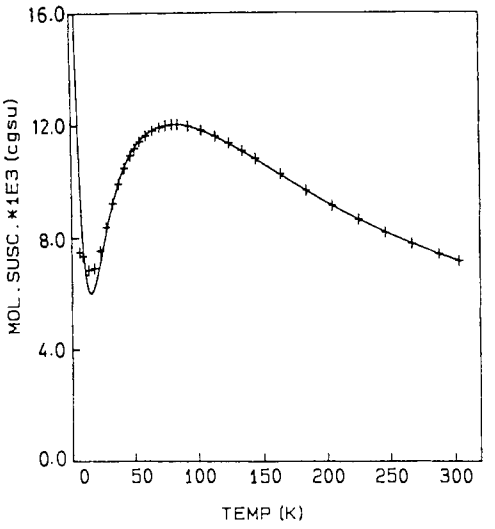

Figure 5. Molar magnetic susceptibility data *vs* temperature for $[Ni_2L(MeOH)_2(ClO_4)_2]\cdot 2NHEt_3ClO_4$ (**3**). The solid line represents the least-squares fit of the data to the theoretical eq 2 given in the text.

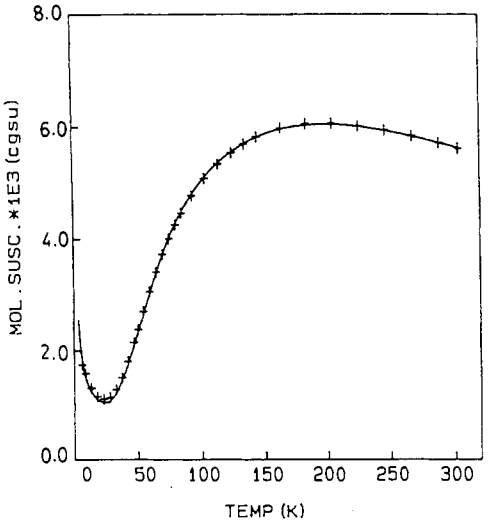

Figure 6. Molar magnetic susceptibility data *vs* temperature for $[Ni_2L(py)_2](ClO_4)_2$ (**5**). The solid line represents the least-squares fit of the data to the theoretical eq 2 given in the text.

(26) The difference in peak potentials ΔE_p, remained unchanged at 70 mV for both the redox couples when scan rate (v) was varied from 50 to 500 mV s^{-1}.

(27) Wen, T.; Thompson, L. K.; Lee, F. L.; Gabe, E. J. *Inorg. Chem.* **1988**, *27*, 4190.

(28) Ginsberg, A. P.; Martin, R. L.; Brookes, R. W.; Sherwood, R. C. *Inorg. Chem.* **1972**, *11*, 2884.

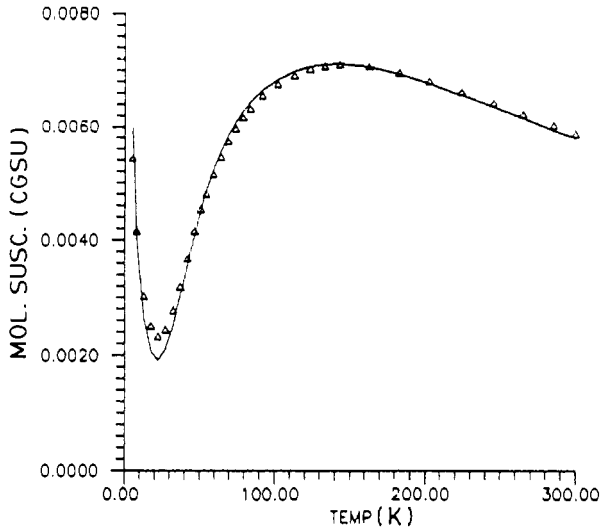

Figure 7. Molar magnetic susceptibility data *vs* temperature for $[Ni_2L(im)_2](ClO_4)_2$ (**4**). The solid line represents the least-squares fit of the data to the theoretical eq 3 given in the text.

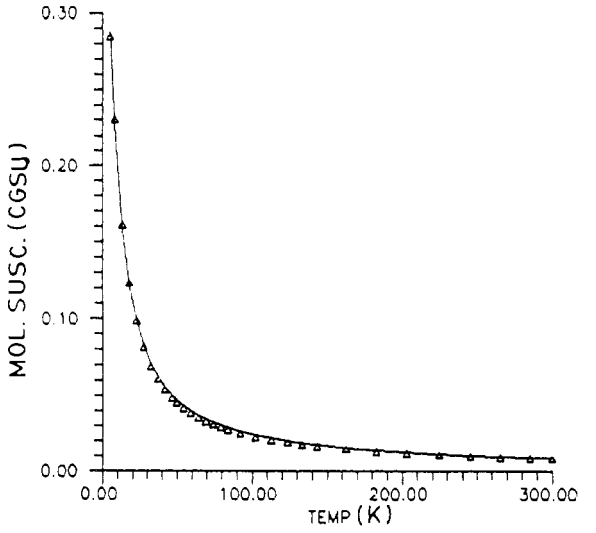

Figure 8. Molar magnetic susceptibility data *vs* temperature for $[Ni_2L(\mu\text{-}O_2CCH_2NH_3)(H_2O)_2](ClO_4)_2{\cdot}2H_2O$ (**6**). The solid line represents the least-squares fit of the data to the theoretical eq 3 given in the text.

has also been used. The molar susceptibility is then given by eq 3.

$$\chi_M = \frac{N\beta^2g^2}{kT}\left[\frac{10 + 2\exp(-4J/kt)}{5 + 3\exp(-4J/kT) + \exp(-6J/kT)}\right](1 - \rho) + \frac{2N\beta^2g^2\rho}{3kT} + N\alpha \quad (3)$$

Nonlinear least-squares fitting of the theoretical expression 2 to the experimental data is illustrated in Figures 4–6 for compounds **2**, **3**, and **5**, respectively. Figures 7 and 8 show the fitting of data for compounds **4** and **6** to eq 3. The relevent magnetic parameters thus obtained are summarized in Table 4. It may be noted that when the same set of susceptibility data is fitted to both expressions 2 and 3 essentially the same J values are obtained; of course, the agreement factor, $R = [\Sigma(\chi_{obs} - \chi_{calcd})^2/\Sigma\chi_{obs}^2]^{1/2}$, is better with eq 2. This vindicates the earlier observation[29] that variation of D and zJ' shows little effect on the evaluation of J because the position of the maxima in the χ_M versus T plot is primarily determined by the coupling constant, J.

(29) Duggan, M. D.; Barefield, E. K.; Hendrickson, D. N. *Inorg. Chem.* **1973**, *12*, 985.

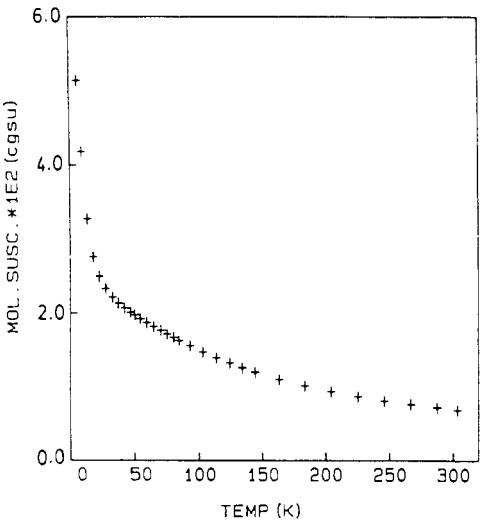

Figure 9. Molar magnetic susceptibility data *vs* temperature for $[Ni_2L(H_2O)_4](ClO_4)_2{\cdot}4NH_2CONH_2$ (**1**).

The χ_M versus T plots shown in Figures 4–7 are typical of binuclear nickel(II) complexes exhibiting significant antiferromagnetic exchange. The temperatures at which maxima in these curves are observed give an idea that the exchange constants of the compounds increase in the following way: **2** (65 K) < **3** (95 K) < **4** (145 K) < **5** (205 K). The susceptibility data for **6** (Figure 8) do not show any peak suggesting weak exchange between the metal centers. Indeed, for this compound the best fit value of J is -1.1 cm^{-1}. The magnetic data for compound **1** (shown in Figure 9) could not be fitted either to eq 2 or eq 3 for the entire temperature range. The χ_M vs T profile gives an impression as if more than one type of exchange interaction is operative or there is a very large contribution due to paramagnetic impurity fractions. The second possibility can be ruled out because highly crystalline specimens with satisfactory analytical data were used for magnetic measurements. Nevertheless, least-squares fitting of the data in the temperature range 50–300 K[30] to expression 3 give $J = -17$ cm^{-1}, $g = 2.15$, $\rho = 0.08$, and $N_\alpha = 4.8 \times 10^{-4}$ cm^{-1} with $R = 3.2 \times 10^{-2}$. The value of J thus obtained appears quite reasonable, although it should be considered as tentative.

The variable-temperature magnetic results (Table 4) of the complexes taken together with their structural parameters (Figure 2) divide them into three groups. Complexes **1**–**3** have octahedral geometric environments for nickel, with a varying degree of tetragonal distortion. The antiferromagnetic exchange in these compounds ($-J$) increases along with the increase in tetragonal distortion: **1** (17 cm^{-1}) < **2** (21 cm^{-1}) < **3** (29 cm^{-1}). For complexes **4** and **5**, in which the metal centers are in square pyramidal environments, there is dramatic increase in the exchange coupling constant with $J = -50$ cm^{-1} for **4** and $J = -67$ cm^{-1} for **5**. By contrast, the two octahedral nickel atoms in **6** are very weakly coupled with $J = -1$ cm^{-1}. The notable structural characteristic of this compound is that the carboxylate bridge is orthogonal to the phenoxide bridge. The dihedral angle between the mean planes of the carboxylate moiety and Ni_2O_2 is 90.2°.

It is worthwhile to consider at this stage the J values reported in literature for other related phenoxo-bridged macrocyclic nickel(II) complexes. For the complex $[Ni_2L'Cl_2]{\cdot}2H_2O$, presumably with square pyramidal geometry for nickel, two J values (−27 and −36 cm^{-1}) have been reported by the same authors.[11a] On

(30) It seems that in the lower temperature regions there is substantial contribution from ferromagnetic coupling. the nature of this ferromagnetic coupling is not clear at this stage, which could be a long-range interaction mediated through the crystal lattice. The molecular structure of **1**[12] shows extensive network of hydrogen bonding involving the adduct urea molecules, perchlorate ions, coordinated water molecules, and amino groups of the macrocyclic ligand.

Table 4. Magnetic Data[a] for the Complexes

compd	J, cm^{-1}	g	zJ', cm^{-1}	D, cm^{-1}	ρ[b]	10^2R[c]
$[Ni_2L(H_2O)_4](ClO_4)_2\cdot 4NH_2CONH_2$ (**1**)	−17.0	2.15			0.08	3.2
$[Ni_2L(NCS)_2(H_2O)_2]\cdot 2Me_2NCHO$ (**2**)	−21.3	2.19	2.0	1.9	0.00006	0.57
	−21.5	2.20			0.0049	1.95
$[Ni_2L(MeOH)_2(ClO_4)_2]\cdot 2NHEt_3ClO_4$ (**3**)	−29.5	2.29	−4.7	29.9	0.023	0.43
	−28.5	2.21			0.046	5.65
$[Ni_2L(im)_2](ClO_4)_2$ (**4**)	−49.8	2.21			0.024	3.37
$[Ni_2L(py)_2](ClO_4)_2$ (**5**)	−67.1	2.24	6.9	22.8	0.003	0.27
	−65.9	2.32			0.008	2.85
$[Ni_2L(\mu\text{-}O_2CCH_2NH_3)(H_2O)_2](ClO_4)_2\cdot 2H_2O$ (**6**)	−1.1	2.21			0.0002	2.25

[a] The results in the first row were obtained from least-squares fitting to eq 2, and those in the second row were obtained from least-squares fitting to eq 3. [b] Fraction of paramagnetic impurity. [c] $R = [\sum(\chi_{obs} - \chi_{calc})^2/\sum\chi_{obs}^2]^{1/2}$.

the other hand, for the octahedral complex $[Ni_2L(py)_4](BF_4)_2$, they have reported[11b] $J = -23$ cm^{-1}. Thus, if we consider $J = -36$ cm^{-1} is the true value for the square pyramidal complex, then the two Ni^{2+} ions in this case are more strongly antiferromagnetically coupled relative to that in the octahedral complex.

The J values of complexes **1–3** and **5** (Table 4) vis-a-vis their structural parameters (Figure 2) qualitatively discern a correlation between the exchange parameters and Ni···Ni distances or Ni–O–Ni bridge angles (θ). The antiferromagnetic exchange interaction appears to increase with the increase of the bridge angle involved in the superexchange pathway. Complex **6**, whose structure is different from the other complexes, does not follow this trend. A more definitive correlation between J and θ can be expected with the availability of more structural data. Presently, the important aspect that has emerged from this study is the dependence of the exchange parameter on the stereochemistry of the metal centers. It transpires that the antiferromagnetic coupling gets augmented with the increase in bond lengths of one of the axial bonds in the hexacoordinate complexes. Substantial increase in the value of $-J$ occurs when a tetragonally elongated six-coordinate species transforms to a five-coordinate square pyramidal species.

As compared to **I–III** and **V**, all of which are centrosymmetric structures, **VI** is unusual with two quite different Ni–O–Ni bridge angles of dissimilar Ni–O distances and an axial carboxylate bridge. Due to these special structural features the magnetic exchange interactions in **6** are more involved. The small magnitude to J_{eff} for **6** (−1.1 cm^{-1}) indicates that further tuning of spin exchange in complexes of this sort should be possible through variation of structural parameters. Indeed, our preliminary studies[31] with a number of carboxylate derivatives have indicated that the value of J_{eff} can be varied between +8 and −5 cm^{-1}.

In conclusion, the wide variation of exchange parameter ranging between −1 and −67 cm^{-1} as reported here is unprecedented in any series of binuclear nickel(II) complexes. This has been achieved simply by changing the auxiliary axial ligands. Needless to say, further tuning of J should be possible by judicious choice of other axial ligands.

Acknowledgment. Thanks are due to the Science and Engineering Research Council, Department of Science and Technology, Government of India, New Delhi, for financial support to this program (to K.N.) and to the Natural Sciences and Engineering Research Council of Canada for the variable-temperature magnetic measurement facility (to L.K.T.).

Supplementary Material Available: Listings of anisotropic thermal parameters for **2** (Table S1), bond lengths and angles pertaining to the ligand in **2** (Table S2), hydrogen atom coordinates for **2** (Table S3), and variable-temperature magnetic susceptibility data for compounds **1–6** (Tables S4–S9) (9 pages). Ordering information is given on any current masthead page.

(31) Nanda, K. K.; Das, R.; Thompson, L. K.; Vankatsubramanian, K.; Nag, K. Unpublished results.